ChemCatChem

ChemCatChem
Chemistry Europe
European Chemical Societies Publishing

RESEARCH ARTICLE OPEN ACCESS

Particle Size Effects in Au/TiO_2 Catalysts for the Oxidation of 5-Hydroxymethylfurfural

Hidde L. Nolten[1] | Marijn A. van Huis[2] | Petra E. de Jongh[3]

[1]Materials Chemistry and Catalysis, Institute for Sustainable and Circular Chemistry, Utrecht University, Utrecht, The Netherlands | [2]Soft Condensed Matter and Biophysics, Debye Institute for Nanomaterials Science, Utrecht University, Utrecht, The Netherlands | [3]Materials Chemistry and Catalysis, Debye Institute for Nanomaterials Science, Institute for Sustainable and Circular Chemistry, Utrecht University, Utrecht, The Netherlands

Correspondence: Petra E. de Jongh (p.e.dejongh@uu.nl)

Received: 8 January 2026 | **Revised:** 28 February 2026 | **Accepted:** 5 March 2026

Keywords: biomass valorization | gold catalysts | liquid phase catalysis | particle size effects | selective oxidation

ABSTRACT

Gold nanoparticles are great catalysts for selective hydrogenation and oxidation reactions, such as for the oxidation of 5-hydroxymethylfurfural (HMF) to 2,5-furandicarboxylic acid, an important reaction in the production of bio-based polymers and an excellent model reaction to evaluate alcohol and aldehyde oxidation performance. The gold particle size is crucial for catalytic applications, but its role in HMF and other liquid-phase oxidation reactions remains insufficiently understood. We report gold particle sizes between 2 and 20 nm within a series of Au/TiO_2 catalysts, made by deposition precipitation with varying heat treatment conditions and precipitation agents. Gold particles larger than 3 nm exhibit good stability, in contrast to even smaller particles that suffer from particle growth, which we attributed to increased solubility probability. The oxidation rate of the alcohol and aldehyde group of HMF depends on the gold particle size, as oxidation rates of both groups decreased with increasing gold particle size. Our 4 nm Au/TiO_2 catalyst outperformed catalysts containing larger gold particle sizes with 2.5 times faster HMF oxidation and 2 times faster oxidation rate of the intermediate 5-hydroxymethyl-2-furancarboxylic acid. Altogether, this paper contributes to the field of gold catalysts in selective oxidation reactions, leading to more rational catalyst design.

1 | Introduction

Selective oxidation reactions are crucial in the chemical industry, making up 30% of all chemical conversions [1]. Selective oxidation allows us to make important organic molecules such as alcohols, aldehydes, carboxylic acids, ketones, and epoxides. It is also crucial in the production of valuable products in sustainable chemical processes, such as biomass valorization, CO oxidation, and catalytic upgrading of methane and other hydrocarbons [2]. Recently, oxidation of alcohols to carboxylic acids has received much interest, as this conversion is pivotal in the production of food additives, pharmaceutics, polymers, and cosmetics [1]. For alcohol to carboxylic acid oxidation, alcohol oxidation is not the only important step, as the subsequently formed ketone or aldehyde should also undergo catalytic oxidation to make carboxylic acids [3]. If the latter is desired, a catalyst in this process ideally catalyzes both.

An intriguing model compound for the oxidation of alcohols and aldehydes is 5-hydroxymethylfurfural (HMF), as this furan molecule possesses both functional groups [3]. Furthermore, HMF is listed as one of the most valuable biomass platform molecules, since it can be converted into many valuable products, like 2,5-furandicarboxylic acid (FDCA), which can be used to replace terephthalic acid in polymer fabrication [4]. The implementation of heterogeneous catalysts in liquid alcohol oxidation is challenging, as the conditions are challenging for their stability [5]. However, heterogeneous catalysts have the

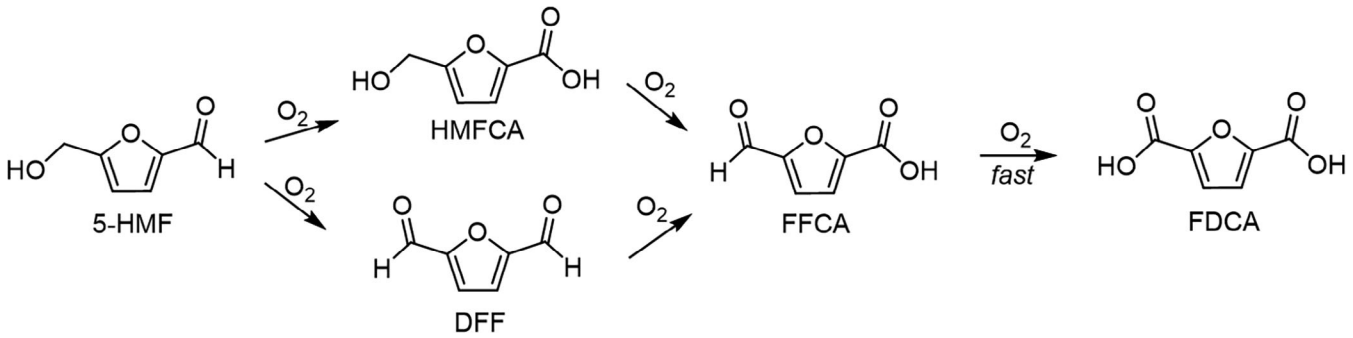

SCHEME 1 | The aerobic oxidation of 5-hydroxymethylfurfural to 2,5-furandicarboxylic acid over two likely pathways.

potential to circumvent the continuous need for stoichiometric amounts of oxidizing reagents in liquid phase oxidation processes that come with high toxicity, continuous waste generation, and costs, but they also allow much more facile separation from the reaction products [6]. Noble metal catalysts are promising catalysts for HMF oxidation, as they offer good corrosion and poisoning resistance [7–11]. Especially gold has received interest, as it is less prone to corrosion and metal leaching than other noble metals, like Pd, Pt, and Ru [12–15]. However, particle growth has also been observed frequently for gold particles in HMF oxidation [16–18]. The growth of particles lowers the active metal surface area, but can also induce other particle size effects [19, 20].

Gold catalysts often exhibit good activity in HMF oxidation, but show limited FDCA production due to slower conversion of the alcohol group [10, 11]. In Scheme 1, two common pathways are depicted, showing that HMF can either be converted to 5-hydroxymethyl-2-furancarboxylic acid (HMFCA) or 2,5-diformylfuran (DFF). Both the conversion of the alcohol and aldehyde have been reported as first-order reactions in HMF and HMFCA, which are both rate-limited by C-H activation [21–25]. This dehydrogenation step is catalyzed by adsorbed hydroxyl ions that also serve as an oxygen source [26, 27]. The catalyst's parameters and reaction conditions determine the surface coverage of hydroxyl ions and reactants, thus affecting both the reaction rate and selectivity toward preferential aldehyde or alcohol conversion.

Specifically for gold catalysts, activity in chemical reactions is often found in small (< 10 nm) nanoparticles; their catalytic activity was only revealed when particles approached the nanoscale [28–31]. Changes in the gold particle size have been reported to result in several effects, impacting catalysis. As particles become smaller than approximately 10 nm, their electronic band structure will consist of a lower density of states around the Fermi level, giving rise to unique electronic and thereby catalytic properties [32, 33]. This is especially important for gold catalysts, as the d-band of macroscopic gold lies well below the Fermi level. As gold particles become smaller, the d band will approach the Fermi level, leading to higher reactivity [34]. It also means that small gold clusters are much more easily oxidized [35, 36]. Besides electronic effects, geometric effects often arise. As the particle size decreases, the fraction of surface atoms increases, and the surface atom distribution shifts from predominantly facet sites to a higher fraction of corner and edge sites [37, 38]. Lastly, the amount and angle of the support-metal interface change as a function of the particle size and are reported as a possible active site in multiple reactions [35, 39, 40]. Investigating the structure-sensitivity of a reaction by changing the metal particle size can provide insights about the active site, as has been done before for Au [19, 41], Ag [42], Pd [43], Pt [44], Ru [45], etc., in oxidation reactions.

In CO oxidation, the highest activities are found for the smallest gold nanoparticles, rhyming with the relative abundance of corner sites, and interface area with the support [41, 46]. Herein, the activation of oxygen is regarded as the rate-limiting step, which is likely to take place on gold-support interface sites [47]. CO adsorbs generally the strongest on corner sites due to their lower coordination number [46, 48]. Moreover, small gold particles often exhibited superior activity in reactions with small molecules, such as CO, H_2, O_2, and NO. However, larger optimal particle sizes were found for gold catalysts in the conversion of larger molecules, as these often need larger surfaces to adsorb on [49–51]. In glucose oxidation, Megías-Sayago et al. [52]. demonstrated that 9 nm particles exhibited the highest TOF, which was explained by improved glucose adsorption. In benzyl alcohol oxidation, 7 nm gold particles exhibited the highest activity [31]. Also, in hydrogenation reactions, improved adsorption of large substrates on larger Au particles was reported [50, 51].

A few studies have reported on the gold particle size effect in HMF. Megías-Sayago et al. [19] investigated 5–40 nm gold particles on a carbon support. They found that smaller (< 10 nm) particles had improved FDCA selectivity compared to particles larger than 10 nm, albeit displaying full conversion of HMF for every catalyst. Schade et al. [20] looked into the effect of the gold particle size distribution on HMF oxidation using 2.1–2.9 nm Au/ZrO_2 catalysts. They suggest that the rate-limiting alcohol oxidation step occurs on large Au crystallites, after which the aldehyde product is converted over the small Au clusters.

We add crucial new insights on the Au particle size effect in HMF oxidation with a systematic approach: First, we use a gold particle size range from 2 to 20 nm on a TiO_2 support for HMF oxidation. An investigation of this range is still lacking, even though it encompasses the range where most particle size effects are expected to occur. Moreover, we provide information on the stability of the gold catalysts during liquid phase oxidation by looking at the particle size with XRD and HAADF-STEM before

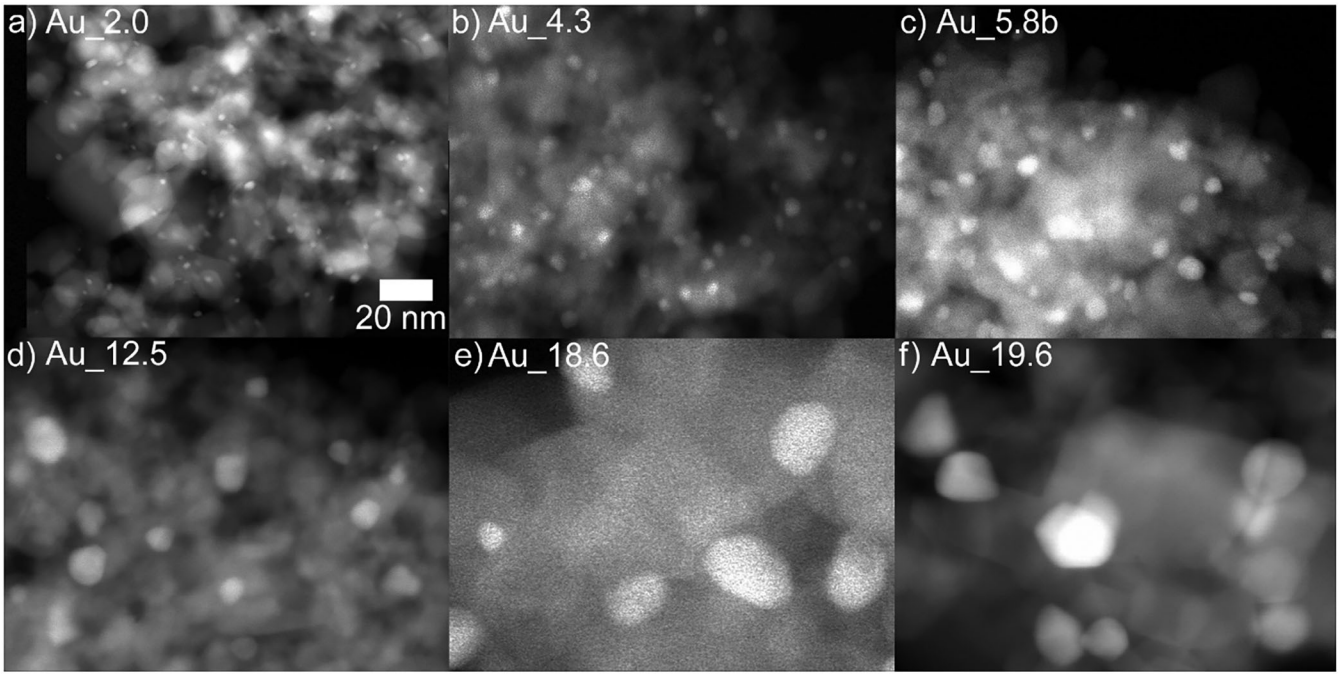

FIGURE 1 | HAADF-STEM images of a series of Au/TiO_2 catalysts with varying Au particle size from 2 to 20 nm, namely (a) Au_2.0, (b) Au_4.3, (c) Au_5,8b, (d) Au_12.5, (e) Au_18.6 and (f) Au_19.6. The scale shown in a) applies to all frames.

and after catalysis. Secondly, we follow the evolution of products of HMF oxidation and its derivatives in time. Earlier research focused solely on the final product distribution, and neither of the mentioned reports includes kinetic studies. Lastly, particle size effects might well be expected to differ between the two reaction steps. Therefore, we report the gold particle size effect in the oxidation of intermediate HMFCA separately, which, to the best of our knowledge, has not been published before. This also yields important information about the activation mechanism of HMFCA compared to HMF.

2 | Results and Discussion

2.1 | Preparation and Characterization of Au/TiO_2 Catalysts With Different Au Particle Sizes

To assess the influence of the gold particle size in HMF oxidation, a series of Au/TiO_2 catalysts with different gold particle sizes was synthesized. The temperature of the calcination treatment after deposition precipitation was adjusted to acquire different gold particle sizes. HAADF-STEM images of selected catalysts can be found in Figure 1a–f. Table 1 displays an overview of all catalysts including relevant structural properties. The Au/TiO_2 catalysts have surface-averaged particle sizes ranging from 2 to 20 nm. NaOH as base was used to precipitate and prepare the Au/TiO_2 catalysts with a particle size of 2.0 and 2.8 nm, listed in Table 1 and displayed in Figure 1a. Deposition precipitation with urea yielded Au/TiO_2 catalysts with particles of 3.8 nm and larger. Using both deposition precipitation methods, the complete series of Au/TiO_2 catalysts was synthesized, covering a wide distribution of particle sizes, between 2 and 20 nm. These catalysts are denoted as Au_X.X, with X.X being the surface-averaged particle diameter. X-Ray Diffraction (XRD) measurements were performed to characterize the average gold crystallite size. In Figures 2 X-Ray diffractograms of selected Au/TiO_2 catalysts are shown. The full overview is presented in Figure S1. The Au(200) peak at 20° for a fcc crystalline structure was used to determine the crystallite sizes, as the Au(111) signal overlaps with a diffraction peak of the TiO_2 support, consisting of approximately of 80% anatase and 20% rutile. Figure 2b clearly illustrates that the Au(200) reflection becomes more pronounced and sharper with growing particle size. Resulting crystallite sizes are displayed in Table 1 and agree well with the TEM data, also shown in Table S1 using volume-weighted particle sizes. It was not possible to determine the average crystallite size of Au/TiO_2 catalysts with particles smaller than 5 nm.

XRD also reveals that the heat treatment affects the TiO_2 crystal phase, as Au_18.6 and Au_19.6 possess a higher rutile content, which is the more stable crystal phase of TiO_2 at this temperature [53]. Unfortunately, the rutile(210) signal interferes with the Au(200) signal, which is why this peak was deconvoluted (Figure S2 and Table S2) to obtain more accurate crystallite sizes for Au_18.6 and Au_19.6, which was validated with the crystallite size, calculated from the Au(111) reflection.

2.2 | Particle Size Stability

An important aspect to be considered when assessing the particle size effect in catalysis is stability. Figure 3 shows the HAADF-STEM-derived surface-averaged particle sizes after 6 h of catalysis compared to particle sizes before entering the reactor. The red dotted line represents the situation in which no particle size growth or shrinkage has taken place. Most catalysts are close to the red line and therefore experienced little overall change in the particle size during catalysis. Only two catalysts diverge

TABLE 1 | Overview of selected Au/TiO_2 catalysts that were tested for HMF oxidation performance.

Catalyst	Synthesis technique	Heat treatment T (°C); and time (h)[a]	Au weight loading (wt.%)[b]	TEM diameter $d_{,TEM, s.a.}$ (nm)[c]	XRD crystallite size d_{XRD} (nm)[d]
Au_2.0	DP NaOH	300; 4	0.58	2.0 ± 0.6	n.a.
Au_2.8	DP NaOH	300; 4	0.48	2.8 ± 0.7	n.a.
Au_3.8	DPU	200; 4	1.65	3.8 ± 1.1	n.a.
Au_4.0	DPU	300; 4	1.49	4.0 ± 1.1	n.a.
Au_4.3	DPU	300; 4	1.65	4.3 ± 0.9	n.a.
Au_5.8a	DPU	550; 4	3.41	5.8 ± 1.3	5.2
Au_5.8b	DPU	525; 6	3.99	5.8 ± 1.3	5.6
Au_12.5	DPU	540; 6	3.75	12.5 ± 2.8	8.3
Au_18.6	DPU	550; 6	3.60	18.6 ± 6.2	9.2
Au_19.6	DPU	600; 10	4.33	19.6 ± 5.4	10.8

[a]All heat treatments were done in synthetic air (20 vol% O_2 in N_2) mixture with a flow rate of 100 $mLmin^{-1}g_{cat}^{-1}$.
[b]Determined from ICP-OES measurements.
[c]Surface-averaged particle diameter and standard deviation from STEM measurements as described in experimental section.
[d]Derived from Scherrer equation on the Au (200) peak.

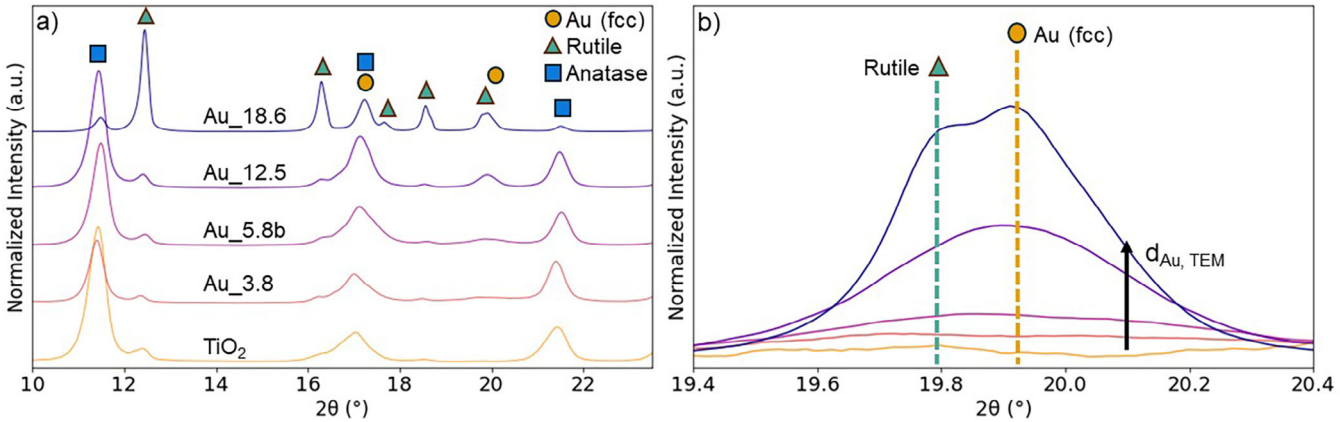

FIGURE 2 | (a) X-Ray diffractograms in the range of 2θ between 10 and 23.5° of selected Au/TiO_2 catalysts with y-offset, obtained using a Mo-K_α source (0.71 Å). The diffractograms are normalized to the maximum. In the top row, theoretical reference XRD reflections are indicated. (b) Zoom-in of the 19.4–20.4° region with increasing intensity and sharper appearance of the Au(200) signal with increasing gold particle size.

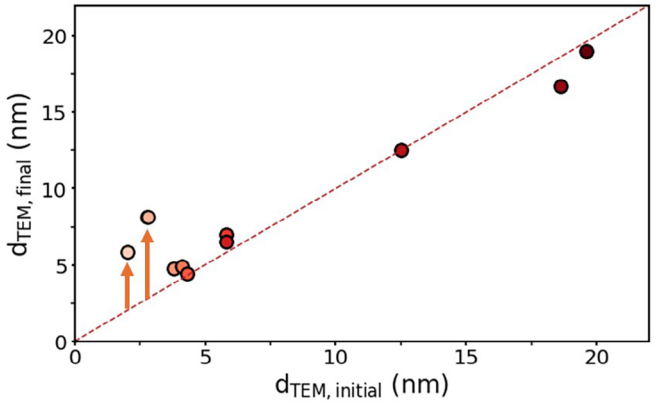

FIGURE 3 | The surface-averaged particle diameter found for all tested Au/TiO_2 catalysts before entering the autoclave reactor and after 6 h of catalysis, determined by measuring at least 200 particles in three different locations using HAADF-STEM images.

significantly from this line, which are the Au/TiO_2 catalysts with the smallest starting particle sizes: Au_2.0 and Au_2.8. These two catalysts grew to 5.8 and 8.2 nm, respectively, which is remarkable as these average final particle sizes exceed those of the average final particle sizes of catalysts starting at averages around 4 to 5 nm. An overview of the exact particle sizes before and after catalysis can be found in Table S3. The particle sizes after catalysis were further confirmed by x-ray diffraction, shown in Figure S3.

To look more closely into the anomalous particle growth of Au_2.8, samples at different stages of catalysis were investigated with HAADF-STEM (Figure 4). Au_2.8 starts at a very small nanoparticle size at an average of 2.8 nm before entering the autoclave in Figure 4a, but has much larger particles after 6 h of catalysis, as can be seen in Figure 4b. This difference is clearly illustrated in the particle size distributions, shown in Figure 4c. Moreover, Figure S4 shows that Au_2.8 has grown

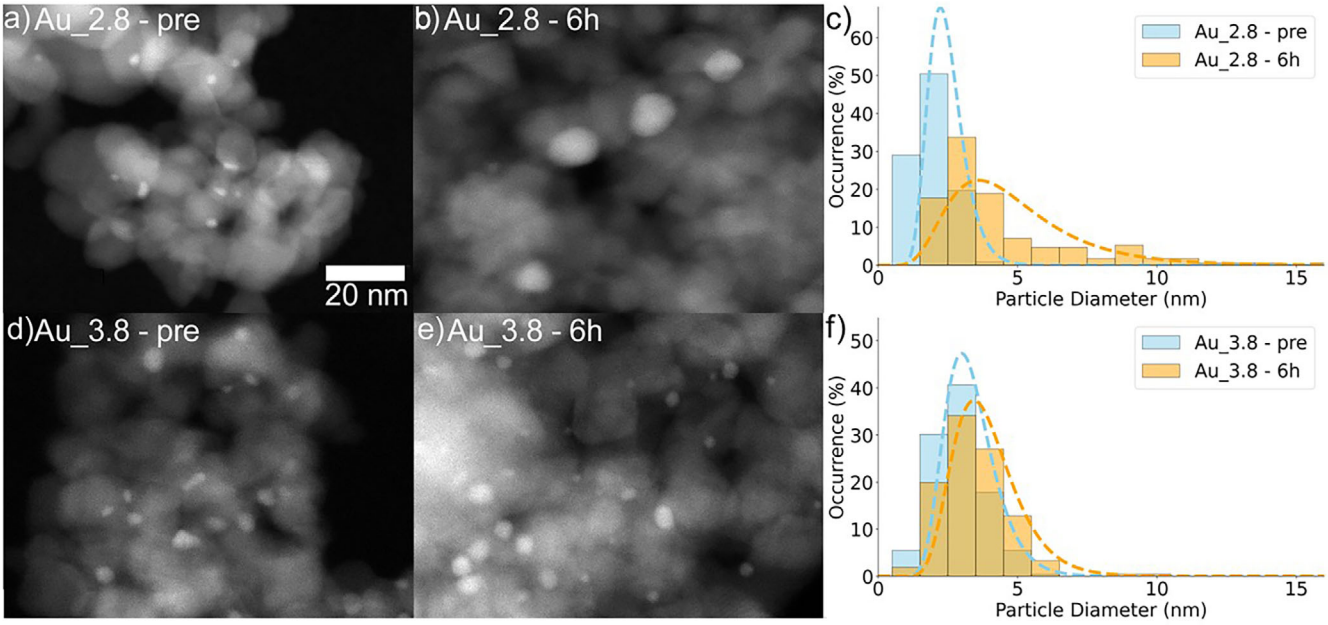

FIGURE 4 | HAADF-STEM images of Au_2.8 and Au_3.8 taken at different stages during catalysis. For Au_2.8 images are shown before entering the autoclave (a) and after 6 h of HMF oxidation at 80°C and 10 bar of O_2 (b). The corresponding particle size distributions are shown in (c). For Au_3.8, only HAADF-STEM images of the catalyst before (d) and after autoclave (e) are presented. The corresponding particle size distributions are shown in (f).

significantly during the autoclave heat-up procedure to 80°C under an atmospheric pressure of N_2. This clearly illustrates that most particle growth of Au_2.8 has taken place before catalytic measurements had even started. As a reference, the next-smallest gold nanoparticle catalyst, Au_3.8, can be seen prior to catalysis in Figure 4d and after 6 h of catalysis in Figure 4e. The STEM images and particle size distributions (Figure 4f) look much alike, indicating a limited effect of catalysis on the particle size of this catalyst. Similar behavior was observed for all other catalysts with particle sizes larger than 3.8 nm.

A possible mechanism for the observed particle growth might be the (partial) detachment of small Au particles from the support. It is well-known that charge-transfer effects take place between TiO_2 support and 1–3 nm gold particles, but this effect becomes less apparent for larger gold crystallites [54]. The charge-transfer can result in a slightly more electropositive nature of small gold particles, resulting in more facile dissolution in the reaction media. The overall observed growth is likely caused by preferential redeposition of detached gold clusters on existing supported gold particles [55]. Similar particle growth behavior was observed for Ni particles in aqueous environments that tend to grow by Ostwald's ripening [56]. Although Au is more corrosion-resistant than Ni, slightly positive charges were reported on small Au particles [35, 36]. This slightly positive charge, enhanced by charge transfer from the TiO_2 support, results in easier detachment or a higher dissolving probability of 1-3 nm gold particles than larger particles. Our limit of 3 nm agrees very well with the metallic to non-metallic behavior transition of supported gold particles, as described by Haruta [35] and Bond [36]. In earlier HMF oxidation research, the presence of organics was listed as a possible reason for particles dissolving or detaching [57, 58]. However, Figure S5 shows that similar particle growth takes place without additional organic components present. The mechanically stirred and pressurized alkaline aqueous media at 80°C evidently allow particle growth, but only for 1–3 nm gold particles.

ICP-OES was performed on filtered reaction solutions after 6 h of catalysis to detect dissolution or suspension of Au_2.8 and Au_18.6. The results are shown in Table S4. Small amounts of dissolved gold were found in the reaction solution. For Au_2.8, 3.3% of the total gold amount was found in the reaction solution, which is much higher than 0.8% for Au_18.6. This showcases a higher leaching probability of gold particles with a size below 3 nm during HMF oxidation.

Because the nanoparticle size changed for the smallest two samples before catalysis, samples were collected, and the catalysis results are related to the surface-averaged nanoparticle size after 6 h of catalysis, instead of the nanoparticle size prior to entering the autoclave, since this is more representative of the particle size during catalysis.

2.3 | HMF Oxidation Performance

The as-prepared catalysts were tested for their performance in HMF oxidation. An example of a typical reaction profile is presented in Figure 5. In the reaction profile, the concentrations of four different molecules as a function of time are shown. First, the aldehyde moiety of HMF is rather quickly converted to a carboxylic acid group in the molecule called HMFCA. The conversion rate of HMF is close to apparent first order in the concentration of HMF (Figure S6). Figure S7 shows an experiment with additional HMFCA and FFCA at the start of a catalysis run. HMF is converted slower when additional experiments are present in the reactor due to competitive adsorption. After the

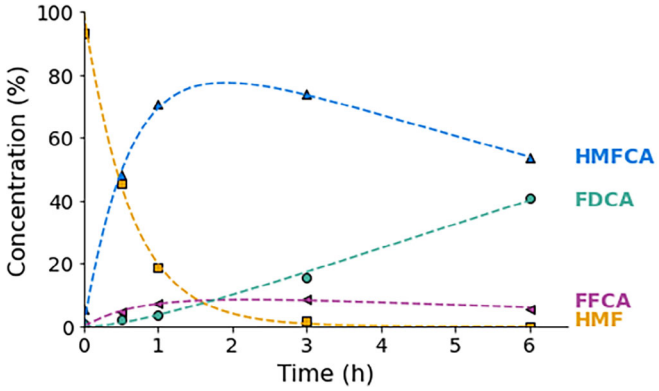

FIGURE 5 | Typical reaction profile of HMF oxidation catalyzed over a Au/TiO_2 catalyst (Au_4.3) with HMF (squares) being converted into FDCA (circles) via HMFCA (triangles facing upwards) and FFCA (triangles facing sideways). The indicators represent data points from HPLC analysis, and the lines are fitted according to kinetic rate equations presented in the experimental section. Conditions: HMF (0.025 M, 1 eq.), $NaHCO_3$ (0.05 M, 2 eq) in H_2O, 47.3 mg Au_4.3, O_2 (10 bar) at 80°C, 900 rpm stirring.

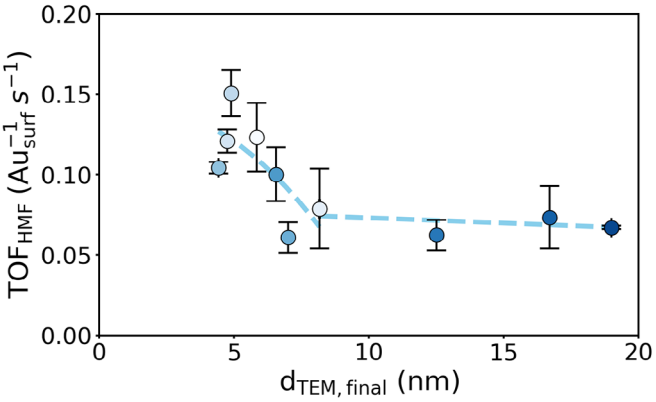

FIGURE 6 | HMF turnover frequency of Au/TiO_2 catalysts as a function of the Au particle size after catalysis with the TOF_{HMF}, based on k_1 from the modeled reaction profile fits. The color gradient of the data points represents the order of the initial particle size, with the larger initial particle sizes being darker. Dashed yellow line is added to guide the eye. All tests were performed under 10 bar O2 and 900 rpm stirring at 80°C in 12 mL milli-Q water filled with 0.025 M HMF, 0.05 M $NaHCO_3$, with varying catalyst loading till a HMF:Au_{surf} ratio of 280:1 was reached.

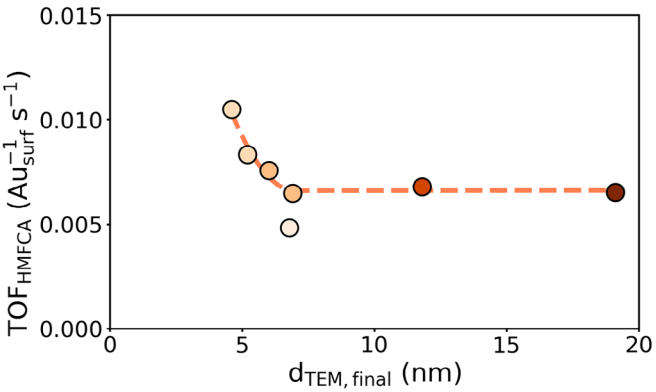

FIGURE 7 | HMFCA turnover frequency of Au/TiO_2 catalysts as a function of the Au particle size after catalysis with a) depicting the TOF_{HMFCA}, based on k_2 from the reaction profile fits. The color gradient of the data points represents the order of the initial particle size, with the larger initial particle sizes being darker. Dashed yellow line is added to guide the eye. All tests were performed under 10 bar O_2 and 900 rpm stirring at 80°C in 12 mL milli-Q water filled with 0.025 M HMFCA, 0.05 M $NaHCO_3$, with varying catalyst loading till a HMFCA:Au_{surf} ratio of 280:1 was reached.

formation of HMFCA, a small amount of FFCA is produced, which is quickly converted to the desired dicarboxylic acid product, FDCA. This reaction profile is in agreement with earlier reported patterns for titania-supported gold catalysts [10, 59]. The conversion of HMFCA usually proceeds slower over gold catalysts than the first oxidation step from HMF to HMFCA. Hence, gold catalysts tend to convert alcohol groups slower than aldehyde groups [10, 11, 59]. The conversion of FFCA occurs very rapidly over gold catalysts, which is evidenced by the low concentrations of FFCA during the catalytic run, which means that the effect on the FDCA production rate can be neglected. The observed activity is only found in the presence of gold nanoparticles, as an identical run with calcined titania did not yield any significant amount of product (Figure S8). Furthermore, homogeneous catalysis was excluded, as hot-filtration tests did not show significant conversion (Figure S9).

In Figure 6, the *TOF* in HMF is displayed as a function of the particle size after catalysis. Error bars in the y-direction indicate the standard deviation between two independent catalysis runs for each catalyst. The results demonstrate a decrease in the TOF_{HMF}, as the nanoparticle size increases. The highest TOF_{HMF} of 0.15 $n_{HMF}Au_{surf}^{-1}s^{-1}$ is observed for Au_4.0, followed by Au_3.8, which are the two catalysts with the smallest stable gold nanoparticle size before catalysis. The five samples with the smallest size after catalysis show the highest TOF_{HMF} values. For catalysts with gold particles larger than 6 nm, a rather constant TOF_{HMF} of around 0.06 $n_{HMF}Au_{surf}^{-1}s^{-1}$ is found. A two-tailed paired t-test indicates that the error in these measurements is smaller than the observed differences (Table S5). Therefore, the conversion of HMF is particle size dependent, with the smallest stable particles of around 4 nm performing best, having a 2.5-fold higher TOF_{HMF} than catalysts having >6 nm particles.

The first product after HMF conversion for gold catalysts is HMFCA, which is converted at a much slower rate than HMF. In Figure S10, the TOF in HMFCA is plotted against the particle size after catalysis. Note that the conversion of HMFCA starts rather late in the measurement, making it more challenging to derive an accurate rate constant. All catalysts tend to follow the same order of preferentially converting all HMF first to HMFCA before producing FFCA and FDCA.

The conversion rate of HMFCA was also measured separately under the same reaction conditions. An overview of the tested catalysts can be found in Table S6. In Figure 7, the TOF_{HMFCA} is displayed as a function of the surface-averaged particle size after catalysis. All catalysts with gold particles ranging from 4 to 20 nm, except one, exhibit TOF_{HMFCA} values ranging from 0.005 to 0.011 $n_{HMFCA}Au_{surf}^{-1}s^{-1}$. The catalyst starting with 2 nm gold particles (the lightest shaded point in Figure 7) exhibits

the lowest TOF_{HMFCA}, which we attribute to a small uncertainty in the particle size after catalysis, as again significant particle growth was observed for gold catalysts starting with particles smaller than 3 nm (Table S6). Catalysts containing gold particles smaller than 7 nm convert HMFCA at an increasingly faster rate with declining particle size, with 4 nm gold particles converting HMFCA the fastest at 0.011 $n_{HMFCA}Au_{surf}^{-1}s^{-1}$. Catalysts containing gold particles larger than 7 nm convert HMFCA at 0.006 $n_{HMFCA}Au_{surf}^{-1}s^{-1}$.

Megías-Sayago et al. also found increased FDCA yield with decreasing gold particle sizes [19]. They argued that it was the FDCA selectivity that was altered upon changing the particle size and not the HMF oxidation rate. Our results agree that the smallest gold particles during catalysis improve the final FDCA yield. However, by disentangling the HMF conversion rate and the HMFCA conversion rate, we show that both alcohol and aldehyde oxidation are particle size dependent and are catalyzed faster by smaller gold nanoparticles.

All catalysts convert HMFCA roughly ten-fold slower than HMF. Inhibition of active sites by other molecules or a reduced base concentration is an unlikely reason, as these experiments started with fresh base and HMFCA in the autoclave reactor. The lower reaction rate is probably due to a much higher thermodynamic energy barrier for C-H activation of alcohols than for aldehydes over gold catalysts [21]. The TOF_{HMFCA} trend follows a similar trend as the observed TOF_{HMF} trend, with catalysts containing particles smaller than 7 nm converting HMFCA at an increasingly faster rate with declining particle size than catalysts containing larger gold particles. This could indicate a similar active site or similar Au catalyst substrate activation mechanism.

Our results show that both the HMF and HMFCA oxidation rates are particle size dependent, with smaller particles converting the substrates at a faster rate. As C—H activation by an adsorbed OH^- is considered the rate-limiting step in both cases, this likely proceeds better with small gold particles. A possible explanation is that gold corner and edge sites serve as the OH^- adsorption site [9, 60]. Activation of small molecules often is easier on smaller gold particles, as their d-band is slightly closer to the Fermi level, resulting in increased activity [32, 33]. Corner and edge sites are more abundant in smaller particles, and these sites have a lower coordination number and therefore an even more quantized electronic band structure. Besides activation and adsorption of base, HMF needs to be adsorbed on the catalyst to be activated by the adsorbed OH^-. This often happens on facets, as HMF is too large to adsorb on one or a few surface atoms only, in agreement with observed trends for glucose, benzyl alcohol, naphthalene, and phenylacetylene adsorption [31, 51, 52, 61]. Therefore, a delicate balance between fractions of corner, edge, and facet atoms is needed for optimal conversion.

Van Hardeveld and Hertog [38] built a model for the expected surface site distributions of fcc crystals. We extrapolated these models (Figure S11) and used them to fit our HMF oxidation rate data. The fits show a combination of facet, corner, and edge sites matches the observed activity trends better than just corner or edge sites (Figure S12). This could mean that this combination of surface sites is responsible for the overall observed activity. However, another structural effect could also play a role in the improved HMF and HMFCA oxidation rates for smaller gold particles. This is the gold-support interface. This interface is mentioned as the oxygen activation and adsorption site in CO oxidation [35, 47]. Therefore, it is likely that this interface can also serve as an adsorption site for OH^- in HMF oxidation. Recent literature in HMF oxidation also suggests that the support plays a major role by serving as an OH^- adsorption site [17, 62]. A closer inspection of the gold-titania interface is shown in Figure S13. High-resolution TEM reveals the contact angles, shapes, and interfaces between various gold particles and the titania carrier (which is a mixture of rutile and anatase phase titania). The conversion rates reported in the present study are a superposition of the interactions taking place at all these structural configurations. In summary, the total amount of metal-support interface increases with decreasing particle size, scaling with our observed increased oxidation rates.

3 | Conclusion

We systematically investigated the Au particle size effect in HMF oxidation over Au/TiO_2 catalysts with particle sizes ranging from 2 to 20 nm. In terms of stability, a strong particle size effect was found using HAADF-STEM and XRD analyses; <3 nm gold particles were more prone to particle growth under the reaction conditions than initially larger particles, resulting in a significant increase in the average particle and crystallite size. 4 nm sized Au particles remained the smallest during catalysis and showed the highest TOF_{HMF}. We explain this by the increased solubility of smaller gold particles due to a more oxidic nature, enhanced by charge-transfer effects of the support. A particle size dependency in HMF oxidation activity was found, indicated by a decreasing TOF_{HMF} from 0.15 to 0.06 n_{HMF} Au_{surf}^{-1} s^{-1} with increasing particle size from 4 to 7 nm after catalysis, after which the TOF_{HMF} was similar for larger Au particles. The TOF_{HMFCA} was determined in separate catalysis runs, revealing a similar trend; 4 nm gold particles to convert HMFCA at 0.01 n_{HMFCA} Au_{surf}^{-1} s^{-1}, faster than 0.006 n_{HMFCA} Au_{surf}^{-1} s^{-1} for gold particles larger than 7 nm. Therefore, both alcohol and aldehyde oxidation are particle size dependent and show higher rates with smaller gold particles. We explain this by improved OH^- adsorption at the more abundant gold-titania interface for increasingly smaller gold particles.

4 | Experimental Section

4.1 | Chemicals

$HAuCl_4.3H_2O$ (≥49.0% Au, ACS reagent, Thermo Fisher Scientific), TiO_2 (90.7 m^2/g, Aeroxide P90, Evonik), NaOH (≥ 99%, pellets for analysis, Sigma–Aldrich), Urea (≥ 99.5%, ACS reagent, Merck), $NaHCO_3$ (≥ 99.7%, ACS reagent, Sigma–Aldrich), 5-hydroxymethylfurfural (≥ 99%, FG, Sigma–Aldrich), 5-hydroxymethyl-2-furancarboxylic acid (Carbosynth)

4.2 | Au/TiO_2 Synthesis

The Au/TiO_2 catalysts were synthesized following the preparation procedure developed by Zanella et al. [63] with slight adjustments. Deposition precipitation using either urea or NaOH as a base was used to obtain Au particles larger than 3 nm and smaller than 3 nm, respectively. For deposition precipitation with urea (DPU), typically 2 g of TiO_2 (P90, Evonik), 100 mL aqueous $HAuCl_4.3H_2O$ (2.0–5.1 mM), and urea (0.42 M) solution were added to a double-wall reactor. The suspension was stirred mechanically at 900 rpm and heated at 80°C for 4 h, after which the suspension was washed 3 times with water and dried at 60°C overnight. Ultimately, a heat treatment procedure was performed in a quartz reactor using a gas flow of 100 mL/g_{cat} 20%/80% O_2/N_2 at varying temperatures for 4 h to obtain Au/TiO_2 with Au particle sizes larger than 3 nm.

Deposition precipitation using NaOH (DPN) was executed to obtain the catalysts with the smallest particle sizes (< 3 nm). In this case, 100 mL of aqueous $HAuCl_4.3H_2O$ solution was added to a round-bottom flask. A few drops of 1 M NaOH solution were added to the flask till a pH of 8 was reached. The solution was heated to 80°C, after which 1 g of TiO_2 was added, and the pH was readjusted to 8 by adding more NaOH solution. This suspension was vigorously stirred and left at 80°C for 24 h, after which it was washed three times with water and dried at 60°C overnight. Ultimately, a heat treatment procedure was performed in a quartz reactor using a gas flow of 100 mL/g_{cat} 20%/80% O_2/N_2 at 300°C for 4 h to obtain Au/TiO_2 with Au particle sizes smaller than 3 nm.

4.3 | Characterization

X-Ray Diffraction measurements were performed on a Malvern Panalytical Empyrean equipped with a Mo K_α radiation source and GaliPIX detector. The diffractograms were recorded from 5 to 40° 2θ with an increment of 0.015°, while mechanically rotated at 15 rpm. The average crystallite size of catalysts was derived from the width of the Au(2 0 0) reflection at 20° by applying the Scherrer equation.

High-angle annular dark-field Scanning Transmission Electron Microscopy (HAADF-STEM) images were captured on a Thermo Fischer Scientific (TFS) TALOS F200X microscope, operating at 200 kV, and on a double aberration-corrected TFS Spectra300, operating at 300 kV, with a probe current of 0.2 nA, and a dwell time of 10 µs. TEM samples were prepared by spreading dry catalyst powder on copper holey carbon grids of 300 µm mesh (Agar Scientific). The average particle size of every catalyst was obtained by manually measuring at least 200 particles in at least 3 different locations on the grid per catalyst using ImageJ software.

Elemental analysis was performed with inductively coupled plasma optical emission spectrometry (ICP-OES) at the Mikroanalytische Laboratorium Kolbe, Germany.

4.4 | Catalytic Testing

The as-made catalysts were added to a PTFE inlet together with 50 mg $NaHCO_3$, 37.8 mg HMF, and 12 mL of milli-Q water. The catalyst loading was adjusted so that one gold surface atom per 280 HMF molecules was present in the solution. This inlet was coupled to a 25 mL stainless steel Parr autoclave. First, the autoclave was flushed five times with nitrogen and subsequently heated under atmospheric pressure to 80°C, whilst stirring at 900 rpm. At 80°C, the autoclave was filled with pure O_2 (99.995%), after which 0.3 mL samples were taken at 0, 0.5, 1, 3, and 6 h. Before every sample, a dummy sample was taken to rinse the tubing.

The catalysis samples were filtered over a 0.45 µm PTFE filter, after which 100 µL was diluted with 400 µL aqueous 17 mM 1-propanol solution as an external standard. These samples were directly measured on a Shimadzu high-performance liquid chromatograph (HPLC) over a Shimadzu Shim-pack SCR 102-H column at 40°C and 0.55 mL/min flow speed. The product concentrations were determined from the measured peak areas compared to a calibration series. For every sample, two HPLC runs were performed, of which the average was taken for further calculations.

Experimentally retrieved data points were fitted using integrated rate equations. From these fits, the rate constants k_1 for HMF conversion and k_2 for HMFCA conversion were derived. We used first-order kinetics, $k_1 >> k'_1$, $k_2 >> k'_2$, and a non-rate-limiting FFCA oxidation.

$$[\boldsymbol{HMF}]_t = [\boldsymbol{HMF}]_0 \cdot \mathbf{e}^{-k_1 \cdot t}$$

$$[\boldsymbol{HMFCA}]_t = [\boldsymbol{HMF}]_0 \cdot \frac{\boldsymbol{k}_1}{(\boldsymbol{k}_2 - \boldsymbol{k}_1)} \cdot (\mathbf{e}^{-k_1 \cdot t} - \mathbf{e}^{-k_2 \cdot t})$$

$$[\boldsymbol{FFCA}]_t = [\boldsymbol{HMF}]_0 \cdot \frac{\mathbf{k}_2}{(\mathbf{k}_3 - \mathbf{k}_2)} \cdot (\mathbf{e}^{-k_2 \cdot t} - \mathbf{e}^{-k_3 \cdot t})$$

$$[\boldsymbol{FDCA}]_t = [\boldsymbol{HMF}]_0 \cdot \left(\left(1 - \frac{\boldsymbol{k}_2}{(\boldsymbol{k}_2 - \boldsymbol{k}_1)} \right) \cdot \mathbf{e}^{-k_1 \cdot t} + \frac{\boldsymbol{k}_1}{(\boldsymbol{k}_2 - \boldsymbol{k}_1)} \cdot \mathbf{e}^{-k_2 \cdot t} \right)$$

The k_1 from the HMF fit was also used in the calculation of the turnover frequency (*TOF*). The *TOF* gives a measure for the intrinsic activity of the catalysts, normalized for the number of gold surface atoms present in the autoclave.

$$\boldsymbol{TOF}_{\mathbf{HMF}} = \frac{\boldsymbol{k}_1 \cdot \boldsymbol{n}_0}{\boldsymbol{n}_{\mathbf{Au-surface\ sites}}}$$

$$\boldsymbol{TOF}_{\mathbf{HMFCA}} = \frac{\boldsymbol{k}_2 \cdot \boldsymbol{n}_0}{\boldsymbol{n}_{\mathbf{Au-surface\ sites}}}$$

The amount of gold surface atoms was calculated using the following formula:

$$\boldsymbol{n}_{\mathbf{Au-surface\ sites}} = \frac{\boldsymbol{m}_{\mathbf{cat}} \cdot \boldsymbol{wt\%Au} \cdot \boldsymbol{D}}{\boldsymbol{M}_{\mathbf{Au}}}$$

Here, m_{cat} stands for the catalyst loading and *wt%Au* for the gold-loading on the catalyst. M_{Au} is the molar mass of gold. Finally, *D* stands for the dispersion and was determined as follows:

$$D = 6 \cdot \frac{V_{Au}/A_{Au}}{d_{TEM,s.a.}}$$

Herein, V_{Au} stands for the volume a gold atom occupies (16.94 Å^3) and A_{Au} for the area a gold atom occupies (8.75 Å^2) [64]. Lastly,

$d_{TEM,s.a}$ stands for the surface-averaged particle size, derived from TEM data and the following formula:

$$d_{\text{TEM, s.a.}} = \frac{\sum n_i d_i^3}{\sum n_i d_i^2}$$

HMFCA oxidation experiments were executed under the same conditions and procedure as described above, but with 42.6 mg of HMFCA instead of HMF. Herein, the HMFCA concentration over time was fitted using the following model:

$$[HMFCA]_t = [HMFCA]_0 \cdot e^{-k_2 \cdot t}$$

Hot-filtration tests were performed using the same conditions as regular HMF oxidation experiments. At $t = 1$ h the catalysis mixture was filtered through a 0.45 µm PTFE filter, after which the reaction was allowed to run for four more hours after re-heating to 80°C.

Acknowledgments

We thank Dennie Wezendonk, Remco Dalebout, and Hans Meeldijk for their technical support. We thank Savannah Turner for helping with atomic-resolution electron microscopy measurements and the Electron Microscopy Centre Utrecht for providing the infrastructure for the microscopes. For access to the Spectra300 electron microscope at Utrecht University, we acknowledge the National Roadmap Infrastructure NEMI, project number 184.034.014, as financed by the Dutch Research Council (NWO). We thank Just Pé Jonasse for critically reading the introduction of the manuscript. We thank Johan de Boed for scientific discussions.

Conflicts of Interest

The authors have no conflicts of interest to declare.

References

1. Z. Guo, B. Liu, Q. Zhang, W. Deng, Y. Wang, and Y. Yang, "Recent Advances in Heterogeneous Selective Oxidation Catalysis for Sustainable Chemistry," *Chemical Society Reviews* 43 (2014): 3480, https://doi.org/10.1039/c3cs60282f.

2. I. Hermans, E. S. Spier, U. Neuenschwander, N. Turrà, and A. Baiker, "Selective Oxidation Catalysis: Opportunities and Challenges," *Topics in Catalysis* 52 (2009): 1162–1174, https://doi.org/10.1007/s11244-009-9268-3.

3. S. E. Davis, M. S. Ide, and R. J. Davis, "Selective Oxidation of Alcohols and Aldehydes Over Supported Metal Nanoparticles," *Green Chemistry* 15 (2013): 17–45.

4. A. Gandini, T. M. Lacerda, A. J. F. Carvalho, and E. Trovatti, "Progress of Polymers from Renewable Resources: Furans, Vegetable Oils, and Polysaccharides," *Chemical Reviews* 116 (2016): 1637–1669.

5. C. Muñoz de Diego, W. Paul Schammel, M. A. Dam, and G. J. M. Gruter, (Furanix Technologies B.V.), US8519167B2, 2013.

6. R. A. Sheldon, "Selective Catalytic Synthesis of Fine Chemicals: Opportunities and Trends," *Journal of Molecular Catalysis A: Chemical* 107 (1996): 75–83, https://doi.org/10.1016/1381-1169(95)00229-4.

7. Y. Ruan, S. Wu, Y. Lu, T. Xu, W. Chen, and W. Lu, "Bidirectional S-Bridge Coordination in the Magnetic Au/FeO_xS_y Catalyst for the Catalytic Oxidation of 5-Hydroxymethylfurfural to 2,5-Furandicarboxylic Acid," *Journal of Materials Chemistry A* 13 (2025): 10814–10824.

8. D. Neukum, M. E. Ludwig, G. Uzunidis, et al., "Synergy of Ag and Pd in Bimetallic Catalysts for the Selective Oxidation of 5-(Hydroxymethyl)Furfural," *Catalysis Science & Technology* 14 (2024): 7163–7171, https://doi.org/10.1039/D4CY01028K.

9. T. Oyegoke, F. Dumeignil, B. E-Yakubu Jibril, C. Michel, and R. Wojcieszak, "Exploring Catalytic Oxidation Pathways of Furfural and 5-Hydroxymethyl Furfural Into Carboxylic Acids Using Au, Pt, and Pd Catalysts: A Comprehensive Review," *Catalysis Science & Technology* 14 (2024): 6761–6774, https://doi.org/10.1039/D4CY00821A.

10. S. E. Davis, L. R. Houk, E. C. Tamargo, A. K. Datye, and R. J. Davis, "Oxidation of 5-Hydroxymethylfurfural Over Supported Pt, Pd and Au Catalysts," *Catalysis Today* 160 (2011): 55–60, https://doi.org/10.1016/j.cattod.2010.06.004.

11. E. J. J. de Boed, H. L. Nolten, N. Masoud, et al., "Effect of Ag Addition to Au Catalysts for the Oxidation of 5-Hydroxymethylfurfural to 2,5-Furandicarboxylic Acid," *Chemcatchem* 16 (2024): e202301436.

12. T. Ståhlberg, E. Eyjólfsdóttir, Y. Y. Gorbanev, I. Sádaba, and A. Riisager, "Aerobic Oxidation of 5-(Hydroxymethyl)Furfural in Ionic Liquids With Solid Ruthenium Hydroxide Catalysts," *Catalysis Letters* 142 (2012): 1089–1097, https://doi.org/10.1007/s10562-012-0858-5.

13. Z. Li, E. Du, P. Hao, et al., "Diluted Oxygen Realizes High Productivity of 2,5-Furandicarboxylic Acid Under Ambient Temperature," *Catalysis Today* 423 (2023): 114277, https://doi.org/10.1016/j.cattod.2023.114277.

14. H. A. Rass, N. Essayem, and M. Besson, "Selective Aerobic Oxidation of 5-HMF Into 2,5-Furandicarboxylic Acid With Pt Catalysts Supported on TiO_2 - and ZrO_2 -Based Supports," *ChemSusChem* 8 (2015): 1206–1217, https://doi.org/10.1002/cssc.201403390.

15. D. Bonincontro, A. Lolli, A. Storione, et al., "Pt and Pt/Sn Carbonyl Clusters as Precursors for the Synthesis of Supported Metal Catalysts for the Base-Free Oxidation of HMF," *Applied Catalysis A: General* 588 (2019): 117279, https://doi.org/10.1016/j.apcata.2019.117279.

16. N. Masoud, B. Donoeva, and P. E. de Jongh, "Stability of Gold Nanocatalysts Supported on Mesoporous Silica for the Oxidation of 5-Hydroxymethyl Furfural to Furan-2,5-Dicarboxylic Acid," *Applied Catalysis A: General* 561 (2018): 150–157, https://doi.org/10.1016/j.apcata.2018.05.027.

17. B. Donoeva, N. Masoud, and P. E. De Jongh, "Carbon Support Surface Effects in the Gold-Catalyzed Oxidation of 5-Hydroxymethylfurfural," *ACS Catalysis* 7 (2017): 4581–4591, https://doi.org/10.1021/acscatal.7b00829.

18. O. R. Schade, F. Stein, S. Reichenberger, et al., "Selective Aerobic Oxidation of 5-(Hydroxymethyl)Furfural Over Heterogeneous Silver-Gold Nanoparticle Catalysts," *Advanced Synthesis & Catalysis* 362 (2020): 5681–5696, https://doi.org/10.1002/adsc.202001003.

19. C. Megías-Sayago, A. Lolli, D. Bonincontro, et al., "Effect of Gold Particles Size over Au/C Catalyst Selectivity in HMF Oxidation Reaction," *ChemCatChem* 12 (2020): 1177–1183, https://doi.org/10.1002/cctc.201901742.

20. O. Schade, P. Dolcet, A. Nefedov, et al., "The Influence of the Gold Particle Size on the Catalytic Oxidation of 5-(Hydroxymethyl)furfural," *Catalysts* 10 (2020): 342–355.

21. B. N. Zope, D. D. Hibbitts, M. Neurock, and R. J. Davis, "During Selective Oxidation Catalysis," *Science* 533 (2010): 74–79.

22. L. Prati, A. Villa, C. E. Chan-Thaw, R. Arrigo, D. Wang, and D. S. Su, "Gold Catalyzed Liquid Phase Oxidation of Alcohol: The Issue of Selectivity," *Faraday Discussions* 152 (2011): 353, https://doi.org/10.1039/c1fd00016k.

23. L. Ardemani, G. Cibin, A. J. Dent, et al., "Solid Base Catalysed 5-HMF Oxidation to 2,5-FDCA Over Au/Hydrotalcites: Fact or Fiction?" *Chemical Science* 6 (2015): 4940–4945, https://doi.org/10.1039/C5SC00854A.

24. W. Yu, Y. Wang, H. Zhang, et al., "Mechanistic Insights Into the Selective Oxidation of 5-Hydroxymethylfurfural Over Au/TiO_2 Catalysts Under Photoexcited and Dark States," *ACS Sustainable Chemistry & Engineering* 11 (2023): 13116–13125, https://doi.org/10.1021/acssuschemeng.3c03289.

25. T. Ji, C. Liu, X. Lu, and J. Zhu, "Coupled Chemical and Thermal Drivers in Microwaves Toward Ultrafast HMF Oxidation to FDCA," *ACS Sustainable Chemistry & Engineering* 6 (2018): 11493–11501, https://doi.org/10.1021/acssuschemeng.8b01630.

26. M. S. Ide and R. J. Davis, "The Important Role of Hydroxyl on Oxidation Catalysis by Gold Nanoparticles," *Accounts of Chemical Research* 47 (2014): 825–833, https://doi.org/10.1021/ar4001907.

27. S. E. Davis, B. N. Zope, and R. J. Davis, "On the Mechanism of Selective Oxidation of 5-Hydroxymethylfurfural to 2,5-Furandicarboxylic Acid Over Supported Pt and Au Catalysts," *Green Chemistry* 14 (2012): 143–147, https://doi.org/10.1039/C1GC16074E.

28. M. Haruta, N. Yamada, T. Kobayashi, and S. Iijima, "Gold Catalysts Prepared by Coprecipitation for Low-Temperature Oxidation of Hydrogen and of Carbon Monoxide," *Journal of Catalysis* 115 (1989): 301–309, https://doi.org/10.1016/0021-9517(89)90034-1.

29. G. J. Hutchings, "Vapor Phase Hydrochlorination of Acetylene: Correlation of Catalytic Activity of Supported Metal Chloride Catalysts," *Journal of Catalysis* 96 (1985): 292–295, https://doi.org/10.1016/0021-9517(85)90383-5.

30. M. Haruta, "Novel Catalysis of Gold Deposited on Metal Oxides," *Catalysis Surveys From Japan* 1 (1997): 61–73.

31. P. Haider, B. Kimmerle, F. Krumeich, W. Kleist, J. D. Grunwaldt, and A. Baiker, "Gold-Catalyzed Aerobic Oxidation of Benzyl Alcohol: Effect of Gold Particle Size on Activity and Selectivity in Different Solvents," *Catalysis Letters* 125 (2008): 169–176, https://doi.org/10.1007/s10562-008-9567-5.

32. G. Schmid, "Large Clusters and Colloids. Metals in the Embryonic State," *Chemical Reviews* 92 (1992): 1709–1727, https://doi.org/10.1021/cr00016a002.

33. P. Claus, A. Bruckner, C. Mohr, and H. Hofmeister, "Supported Gold Nanoparticles From Quantum Dot to Mesoscopic Size Scale: Effect of Electronic and Structural Properties on Catalytic Hydrogenation of Conjugated Functional Groups," *Journal of the American Chemical Society* 122 (2000): 11430–11439, https://doi.org/10.1021/ja0012974.

34. J. A. Van Bokhoven and J. T. Miller, "d Electron Density and Reactivity of the d Band as a Function of Particle Size in Supported Gold Catalysts," *Journal of Physical Chemistry C* 111 (2007): 9245–9249, https://doi.org/10.1021/jp070755t.

35. M. Haruta, "When Gold Is Not Noble: Catalysis by Nanoparticles," *Chemical Record* 3 (2003): 75–87, https://doi.org/10.1002/tcr.10053.

36. G. C. Bond, "The Effect of the Metal to Non-Metal Transition on the Activity of Gold Catalysts," *Faraday Discussions* 152 (2011): 277, https://doi.org/10.1039/c1fd00010a.

37. R. A. van Santen, "Complementary Structure Sensitive and Insensitive Catalytic Relationships," *Accounts of Chemical Research* 42 (2009): 57–66, https://doi.org/10.1021/ar800022m.

38. R. Van Hardeveld and F. Hartog, "The Statistics of Surface Atoms and Surface Sites on Metal Crystals," *Surface Science* 15 (1969): 189–230, https://doi.org/10.1016/0039-6028(69)90148-4.

39. M. Du, D. Sun, H. Yang, et al., "Influence of Au Particle Size on Au/TiO_2 Catalysts for CO Oxidation," *Journal of Physical Chemistry C* 118 (2014): 19150–19157, https://doi.org/10.1021/jp504681f.

40. S. Ichikawa, T. Akita, M. Okumura, M. Haruta, K. Tanaka, and M. Kohyama, "Electron Holographic 3-D Nano-Analysis of Au/TiO_2 Catalyst at Interface," *Journal of Electron Microscopy* 52 (2003): 21–26, https://doi.org/10.1093/jmicro/52.1.21.

41. S. H. Overbury, V. Schwartz, D. R. Mullins, W. Yan, and S. Dai, "Evaluation of the Au Size Effect: CO Oxidation Catalyzed by Au/TiO2," *Journal of Catalysis* 241 (2006): 56–65, https://doi.org/10.1016/j.jcat.2006.04.018.

42. J. E. van den Reijen, S. Kanungo, T. A. J. Welling, et al., "Preparation and Particle Size Effects of Ag/A-Al_2O_3 Catalysts for Ethylene Epoxidation," *Journal of Catalysis* 356 (2017): 65–74, https://doi.org/10.1016/j.jcat.2017.10.001.

43. J. Chen, Q. Zhang, Y. Wang, and H. Wan, "Size-Dependent Catalytic Activity of Supported Palladium Nanoparticles for Aerobic Oxidation of Alcohols," *Advanced Synthesis & Catalysis* 350 (2008): 453–464, https://doi.org/10.1002/adsc.200700350.

44. S. Ge, W. Fan, X. Tang, et al., "Revealing the Size Effect of Ceria Nanocube-Supported Platinum Nanoparticles in Complete Propane Oxidation," *ACS Catalysis* 14 (2024): 2532–2544, https://doi.org/10.1021/acscatal.3c06139.

45. S. H. Joo, J. Y. Park, J. R. Renzas, D. R. Butcher, W. Huang, and G. A. Somorjai, "Size Effect of Ruthenium Nanoparticles in Catalytic Carbon Monoxide Oxidation," *Nano Letters* 10 (2010): 2709–2713, https://doi.org/10.1021/nl101700j.

46. N. Lopez, T. V. W. Janssens, B. S. Clausen, et al., "On the Origin of the Catalytic Activity of Gold Nanoparticles for Low-Temperature CO Oxidation," *Journal of Catalysis* 223 (2004): 232–235, https://doi.org/10.1016/j.jcat.2004.01.001.

47. I. X. Green, W. Tang, M. Neurock, and J. T. Yates, "Spectroscopic Observation of Dual Catalytic Sites during Oxidation of CO on a Au/TiO_2 Catalyst," *Science* 303 (2011): 736–739.

48. T. Jiang, D. J. Mowbray, S. Dobrin, et al., "Trends in CO Oxidation Rates for Metal Nanoparticles and Close-Packed, Stepped, and Kinked Surfaces," *Journal of Physical Chemistry C* 113 (2009): 10548–10553, https://doi.org/10.1021/jp811185g.

49. L. Guczi, A. Beck, and Z. Pászti, "Gold Catalysis: Effect of Particle Size on Reactivity Towards Various Substrates," *Catalysis Today* 181 (2012): 26–32, https://doi.org/10.1016/j.cattod.2011.08.037.

50. J. E. Bailie, H. A. Abdullah, J. A. Anderson, et al., "Hydrogenation of but-2-Enal Over Supported Au/ZnO Catalysts," *Physical Chemistry Chemical Physics* 3 (2001): 4113–4121, https://doi.org/10.1039/b103880j.

51. B. Pawelec, A. M. Venezia, V. La Parola, S. Thomas, and J. L. G. Fierro, "Factors Influencing Selectivity in Naphthalene Hydrogenation Over Au- and Pt–Au-Supported Catalysts," *Applied Catalysis A: General* 283 (2005): 165–175, https://doi.org/10.1016/j.apcata.2005.01.004.

52. C. Megías-Sayago, J. L. Santos, F. Ammari, et al., "Influence of Gold Particle Size in Au/C Catalysts for Base-Free Oxidation of Glucose," *Catalysis Today* 306 (2018): 183–190, https://doi.org/10.1016/j.cattod.2017.01.007.

53. F. De Angelis, C. Di Valentin, S. Fantacci, A. Vittadini, and A. Selloni, "Theoretical Studies on Anatase and Less Common TiO_2Phases: Bulk, Surfaces, and Nanomaterials," *Chemical Reviews* 114 (2014): 9708–9753, https://doi.org/10.1021/cr500055q.

54. V. Subramanian, E. E. Wolf, and P. V. Kamat, "Catalysis with TiO_2 /Gold Nanocomposites. Effect of Metal Particle Size on the Fermi Level Equilibration," *Journal of the American Chemical Society* 126 (2004): 4943–4950, https://doi.org/10.1021/ja0315199.

55. M. J. Meijerink, K. P. De Jong, and J. Zečević, "Growth of Supported Gold Nanoparticles in Aqueous Phase Studied by In Situ Transmission Electron Microscopy," *Journal of Physical Chemistry C* 124 (2020): 2202–2212, https://doi.org/10.1021/acs.jpcc.9b10237.

56. T. Van Haasterecht, M. Swart, K. P. De Jong, and J. H. Bitter, "Effect of Initial Nickel Particle Size on Stability of Nickel Catalysts for Aqueous Phase Reforming," *Journal of Energy Chemistry* 25 (2016): 289–296, https://doi.org/10.1016/j.jechem.2016.01.006.

57. Z. Jamshidi, H. Farhangian, and Z. A. Tehrani, "Glucose Interaction With Au, Ag, and Cu Clusters: Theoretical Investigation," *International Journal of Quantum Chemistry* 113 (2013): 1062–1070, https://doi.org/10.1002/qua.24122.

58. W. Naim, O. R. Schade, E. Saraçi, D. Wüst, A. Kruse, and J. D. Grunwaldt, "Toward an Intensified Process of Biomass-Derived Monomers: the Influence of 5-(Hydroxymethyl)Furfural Byproducts on the Gold-Catalyzed Synthesis of 2,5-Furandicarboxylic Acid," *ACS Sus-*

tainable Chemistry & Engineering 8 (2020): 11512–11521, https://doi.org/10.1021/acssuschemeng.0c01319.

59. O. Casanova, S. Iborra, and A. Corma, "Biomass Into Chemicals: Aerobic Oxidation of 5-Hydroxymethyl-2-Furfural Into 2,5-Furandicarboxylic Acid With Gold Nanoparticle Catalysts," *ChemSusChem* 2 (2009): 1138–1144, https://doi.org/10.1002/cssc.200900137.

60. S. Wang, H. Feng, T. Liu, et al., "Theoretical Exploration of the Origin of Alkaline Dependence in the Oxidation of 5-Hydroxymethylfurfural Catalyzed by NiO_2 H X," *ACS Catalysis* 14 (2024): 9860–9869, https://doi.org/10.1021/acscatal.4c00940.

61. V. K. Kanuru, G. Kyriakou, S. K. Beaumont, A. C. Papageorgiou, D. J. Watson, and R. M. Lambert, "Sonogashira Coupling on an Extended Gold Surface in Vacuo: Reaction of Phenylacetylene With Iodobenzene on Au(111)," *Journal of the American Chemical Society* 132 (2010): 8081–8086, https://doi.org/10.1021/ja1011542.

62. A. Bueno, N. Viar, M. B. Conway, I. Gandarias, J. M. Requies, and M. Sankar, "Aerobic Oxidation of 5-Hydroxymethylfurfural to 2,5-Furandicarboxylic Acid Over Au/Hydrotalcite Catalyst – Role of Support and Synthesis Methodology on the Activity and Stability," *Fuel* 403 (2026): 136088.

63. R. Zanella, S. Giorgio, C. R. Henry, et al., "Alternative Methods for the Preparation of Gold Nanoparticles Supported on TiO_2," *The Journal of Physical Chemistry B* 106 (2002): 7634–7642.

64. G. Bergeret and P. Gallezot, *Handbook of Heterogeneous Catalysis*, ed. G. Ertl, H. Knözinger, F. Schuth, and J. Weitkamp (Wiley-VCH, 1997), 439–464.

Supporting Information

Additional supporting information can be found online in the Supporting Information section.

Supporting File: cctc70676-sup-0001-SuppMat.docx